Bulk and isospin instabilities in hot nuclear matter

V. M. Kolomietz[1] and S. Shlomo[2,3]
[1]*Institute for Nuclear Research, 03680 Kiev, Ukraine*
[2]*Cyclotron Institute, Texas A&M University, College Station, Texas 77843, USA*
[3]*Department of Elementary Particles and Astrophysics, the Weizmann Institute of Science, Rehovot 76100, Israel*
(Received 1 December 2016; revised manuscript received 14 February 2017; published 16 May 2017)

The instability of hot asymmetric nuclear matter with respect to bulk density distortions is considered. The equation of state of the extended Thomas-Fermi approximation is used. The origin of the anomalous dispersion and the influence of the Fermi-surface distortion effects on the bulk and isospin instabilities in homogenous nuclear matter are investigated. It is shown that the development of both instabilities is reduced significantly due to the Fermi-surface distortion effects. The dependence of the bulk instability on the temperature and on the multipolarity of the particle density distortions are shown for the nucleus of ^{208}Pb. The dependence of the formation of the decay modes (fission or multifragmentation) of the nuclei on the temperature and the Fermi-surface distortion effects are demonstrated. It is shown that in the case of low temperatures the preferable mode for the bulk instability is binary fission. For higher temperatures, the preferred modes are the multifragmentations for small clusters. The number of clusters increases with increasing temperature.

DOI: 10.1103/PhysRevC.95.054613

I. INTRODUCTION

Diluted nuclear matter is unstable with respect to particle density fluctuations. One expects that such a kind of bulk instability plays a significant role in internal clusterization and multifragmentation in heavy-ion collisions. The bulk instability of nuclear matter was studied earlier in Refs. [1–8] where the different aspects of the nuclear equation of state (EOS) were taken into consideration.

We note, however, that in actual nuclear processes (heavy-ion reactions, nuclear fission, etc.), the development of instability depends not only on the equation of state, but also on the dynamic effects, such as the dynamic Fermi-surface distortions (FSDs). In particular, the FSD effects lead to collisional relaxation on the distorted Fermi surface and to non-Markovian motion in a viscous nuclear Fermi liquid [9]. In the present paper, we mainly focus on these aspects in studying bulk instability considering the regimes of frequent and rare internucleon collisions.

Some specific difficulties appear in the theoretical description of the instability in an arbitrary dilute many-body system due to the necessity to consider the small density fluctuations around a nonequilibrium state of the system. Usually the nonequilibrium state can be fixed through the introduction of a formal constrained field [10]. Note also that in considering the development of bulk instability in a homogeneous nuclear matter one has to use an EOS, which is extended to include the gradient terms of particle density ρ. That is because the particle density perturbations $\delta\rho(\boldsymbol{r},t)$ are, in general, nonhomogeneous ones. In the present paper we use the EOS, which is based on the semiclassical extended Thomas-Fermi approximation (ETFA), for the internal kinetic energy of the nucleons and the potential energy due to the Skyrme effective nucleon-nucleon interaction. The inclusion of the gradient terms in the EOS leads to a specific effect of the anomalous dispersion which plays a significant role in the description of the instability growth rate in nuclear matter.

The present paper is an extension of our previous work [7] where the general concept of the Fermi motion effects was adopted in studying the bulk instability of nuclear matter. In the present paper we generalize our approach for both the spinodal (bulk) and the isospin instabilities and carry out numerical calculations employing commonly used Skyrme interactions. We pay special attention to the derivation of the stiffness coefficients, such as the incompressibility and isospin symmetry coefficients, beyond the equilibrium point by employing the variational Euler-Lagrange procedure. We analyze the occurrence of the anomalous dispersion in both the isoscalar and the isovector channels. We consider the temperature dependence of the instability growth rate for the bulk mode. We also study the dependence of the instability growth rate on the multipolarity of the nuclear density distortions in hot nuclei with increasing temperature. The last aspect is important since an increase in the temperature strongly reduces the Fermi-surface distortion effects and the relaxation processes and thereby the growth of instabilities. We point out that the use of the Skyrme interaction with parameters adjusted to reproduce the ground-state properties of the nuclei within the mean-field model is a reasonable approximation for our purposes. In fact, the effective interaction is modified only slightly (by a few percent) in a wide temperature range of $T = 0-20$ MeV [11,12].

In Sec. II we describe the fluid dynamic approach to the instability of nuclear matter by using the extended EOS, which includes the gradient corrections to the energy density functional. The approach is based on the extended Thomas-Fermi approximation and the effective Skyrme interactions. In Sec. III we provide numerical results for the instability growth rate and its dependence on the temperature and the multipolarity of the particle density perturbations. Our conclusions are given in Sec. IV.

II. BULK INSTABILITY OF ASYMMETRIC NUCLEAR MATTER

We consider the $\boldsymbol{r}$-dependent density fluctuations $\delta\rho(\boldsymbol{r},t)$ around an arbitrary nonequilibrium density $\rho_0 = \text{const}$ of a

homogeneous nuclear matter. Following the Euler-Lagrange method, the nonequilibrium particle density ρ_0 can be fixed by introducing a formal constrained field into the relevant variational procedure for the total energy E of a many-body system. Employing this method to nuclear matter and assuming the possible $\boldsymbol{r}$ dependence of the particle density ρ, we write its total energy as

$$E = \int d\boldsymbol{r}\ \epsilon_{\rm tot}[\rho], \quad \epsilon_{\rm tot}[\rho] = \epsilon_{\rm kin}[\rho] + \epsilon_{\rm pot}[\rho], \qquad (1)$$

where $\epsilon_{\rm kin}[\rho]$ and $\epsilon_{\rm pot}[\rho]$ are the $\boldsymbol{r}$-dependent kinetic- and potential-energy densities of nuclear matter which are derived below. An arbitrary density ρ_0 is then given by the following variational Euler-Lagrange equation,

$$\frac{\delta}{\delta\rho}\left[\int d\boldsymbol{r}(\epsilon_{\rm tot}[\rho] - \xi\rho)\right]\Bigg|_{\rho=\rho_0} = 0, \qquad (2)$$

where $-\xi\rho$ is the constrained field and ξ is the Lagrange multiplier of the Euler-Lagrange method. Below we use the density ρ_0 as an independent variable, and Eq. (2) is considered as a derivation of the Lagrange multiplier ξ only. The inclusion of the constrained field in the variational procedure of Eq. (2) plays an important conceptual role because it allows us to consider the adiabatic stiffness coefficients beyond the equilibrium point.

In evaluating the potential-energy density $\epsilon_{\rm pot}[\rho]$ in Eq. (1), we adopt the Skyrme-type effective nucleon-nucleon interaction in the following standard form [13–15]:

$$\begin{aligned} v_{12} = {} & t_0\left(1 + x_0 P_{12}^{\sigma}\right)\delta(\boldsymbol{r}_1 - \boldsymbol{r}_2) \\ & + \frac{1}{2}t_1\left(1 + x_1 P_{12}^{\sigma}\right)\left[\overleftarrow{k}_{12}^{2}\,\delta(\boldsymbol{r}_1 - \boldsymbol{r}_2) + \delta(\boldsymbol{r}_1 - \boldsymbol{r}_2)\vec{k}_{12}^{2}\right] \\ & + t_2\left(1 + x_2 P_{12}^{\sigma}\right)\overleftarrow{k}_{12}\,\delta(\boldsymbol{r}_1 - \boldsymbol{r}_2)\vec{k}_{12} \\ & + \frac{1}{6}t_3\left(1 + x_3 P_{12}^{\sigma}\right)\rho^{\nu}\left(\frac{\boldsymbol{r}_1 + \boldsymbol{r}_2}{2}\right)\delta(\boldsymbol{r}_1 - \boldsymbol{r}_2) \\ & + i W_0\,\overleftarrow{k}_{12}\,\delta(\boldsymbol{r}_1 - \boldsymbol{r}_2)(\boldsymbol{\sigma}_1 + \boldsymbol{\sigma}_2)\ \times \vec{k}_{12}. \end{aligned} \qquad (3)$$

where t_i, x_i, ν, and W_0 are the parameters of the interaction, P_{12}^{σ} is the spin-exchange operator, $\boldsymbol{\sigma}_i$ is the Pauli spin operator, $\vec{k}_{12} = -i(\vec{\boldsymbol{\nabla}}_1 - \vec{\boldsymbol{\nabla}}_2)/2$, and $\overleftarrow{k}_{12} = -i(\overleftarrow{\boldsymbol{\nabla}}_1 - \overleftarrow{\boldsymbol{\nabla}}_2)/2$. Here, the right and left arrows indicate that the momentum operators act on the right and on the left, respectively.

In a Fermi liquid, the linearized equation of motion for small variations $\delta\rho = \rho - \rho_0$ of the particle density near arbitrary ρ_0 can be written as, see Refs. [7,9],

$$m\,\frac{\partial^2}{\partial t^2}\,\delta\rho = \boldsymbol{\nabla}\rho_0\,\boldsymbol{\nabla}\frac{\delta E}{\delta\rho}\ + \nabla_\nu\nabla_\mu P'_{\nu\mu}. \qquad (4)$$

The equation of motion (4) is obtained from the kinetic equation for Wigner's distribution function $f \equiv f(\boldsymbol{r},\boldsymbol{p};t)$ and includes both the relaxation phenomena and the Fermi-surface distortion effects [9]. The pressure tensor $P'_{\nu\mu}$ in Eq. (4) is caused by the dynamic distortions of the Fermi surface, see Refs. [9,16,17]. We point out that the constrained field $-\xi\rho$ does not contribute to the equation of motion (4) since $\xi =$ const.

Note that the total energy E of the homogeneous nuclear matter in Eq. (4) is written beyond the point $\rho_0 =$ const. where the particle density $\rho = (\boldsymbol{r},t)$ becomes $\boldsymbol{r}$ dependent. To take this fact into consideration, we use the ETFA for the kinetic-energy density $\epsilon_{\rm kin}[\rho]$ (see Refs. [18,19]) and the density-dependent Skyrme interaction for the potential-energy density $\epsilon_{\rm pot}[\rho]$ [20], which include the gradient terms $\sim\boldsymbol{\nabla}\rho$. Since the values $\epsilon_{\rm kin}[\rho]$ and $\epsilon_{\rm pot}[\rho]$ contain the gradients of the particle density, the evaluation of the functional derivative $\delta E/\delta\rho$ in Eq. (4) must have the form

$$\frac{\delta E}{\delta\rho} = \left[\frac{\partial}{\partial\rho} - \boldsymbol{\nabla}\frac{\partial}{\partial(\boldsymbol{\nabla}\rho)} + \nabla^2\frac{\partial}{\partial(\nabla^2\rho)}\right]\epsilon_{\rm tot}[\rho]. \qquad (5)$$

We consider an asymmetric nuclear matter with asymmetry parameter $X = (N - Z)/(N + Z)$, where N and Z are the number of neutrons and protons, respectively. We introduce the isoscalar density $\rho_+ = \rho_n + \rho_p$ and the neutron excess (isovector) density $\rho_- = \rho_n - \rho_p = X\rho_+$, where ρ_n is the neutron density and ρ_p is the proton density. Below we restrict ourselves to the commonly used case of a small isospin asymmetry $X \ll 1$, which allows one, in particular, to derive the isospin symmetry energy and is sufficient for all existing nuclei. Since $\rho_- \ll \rho_+$, the total energy density $\epsilon_{\rm tot}[\rho]$ can be reduced to the following convenient form, see Appendix, Eqs. (A2) and (A3),

$$\begin{aligned} \epsilon_{\rm tot}[\rho] = {} & A_1(\rho_+) + A_2(\rho_+)\,\rho_-^2 + [B_1(\rho_+) + C_1(\rho_+,\rho_-)] \\ & \times(\boldsymbol{\nabla}\rho_+)^2 + B_2(\rho_+)(\boldsymbol{\nabla}\rho_-)^2 \\ & + D_1(\rho_+,\rho_-)\nabla^2\rho_+, \end{aligned} \qquad (6)$$

where the density-dependent functions $A_i(\rho)$, $B_i(\rho)$, $C_1(\rho)$, and $D_1(\rho)$ are given in Appendix Eq. (A3). The expression (6) is written up to the second order in X. The higher-order correction $\sim X^4$ is negligible in practically all interesting cases.

Using Eqs. (1) and (5), taking pressure tensor $P'_{\nu\mu}$ from Ref. [9], and assuming $\delta\rho \sim \exp[i(qr - \omega t)]$, the equation of motion (4) is transformed to the following form:

$$\begin{aligned} -m\,\omega^2\,\delta\rho_\pm = {} & [C_\pm(\rho_0) - P_{F,\pm}(\rho_0)]\,\nabla^2\delta\rho_\pm \\ & - F_{S,\pm}(\rho_0)\,\nabla^2\nabla^2\delta\rho_\pm. \end{aligned} \qquad (7)$$

Here, the transport coefficients $C_\pm$ and $P_{F,\pm}$ are given by

$$\begin{aligned} C_+(\rho_0) &= \frac{K(\rho_0)}{9}, \quad C_-(\rho_0) = 2C_{\rm sym}(\rho_0), \\ P_{F,\pm}(\rho_0) &= \frac{4}{3}\frac{i\omega\tau_\pm}{1 - i\omega\tau_\pm}\left(\frac{P_0}{\rho_0}\right), \end{aligned} \qquad (8)$$

where P_0 is the pressure $P_0 = \rho_0\,p_F^2/5\,m$, p_F is the Fermi momentum, and $\tau_\pm$ is the relaxation time, which can be different for isoscalar and isovector channels [21]. The transport coefficients $F_{S,\pm}$ in Eq. (7) are the coefficients of the anomalous dispersion which play a significant role in the case of short-wavelength density fluctuations.

Taking into account the finite temperature, we use the adiabatic (isentropic) [22] values of transport coefficients in Eq. (7). Using Eqs. (7) and (A4) and (A5) of the Appendix, one obtains for the isoscalar mode the incompressibility

coefficient,

$$K(\rho_0) = 10\,\alpha\,\frac{\hbar^2}{2m}\rho_0^{2/3} + \frac{27}{4}t_0\rho_0 + \frac{9}{16}(2+\nu)(1+\nu)t_3\rho_0^{1+\nu} + 10\,\alpha\left(\frac{3t_1+5t_2}{4} + t_2x_2\right)\rho_0^{5/3} + X^2\left[\frac{10}{9}\alpha\frac{\hbar^2}{2m}\rho_0^{4/3} + \frac{3}{8}\nu(\nu-1)t_3\left(x_3+\frac{1}{2}\right)\rho_0^{\nu+1} - \frac{10}{9}\alpha\left(\frac{t_2}{2} + \frac{5t_2x_2 - 3t_1x_1}{8}\right)\rho_0^{5/3}\right], \quad (9)$$

and the isoscalar coefficient of the anomalous dispersion,

$$F_{S,+}(\rho_0) = \frac{1}{2}\frac{\hbar^2}{2m}\eta + \left[\frac{1}{6}t_1 - \frac{25}{72}t_2\left(1+\frac{4}{5}x_2\right)\right]\rho_0 - X^2\left\{\frac{1}{2}\frac{\hbar^2}{2m}\eta + \frac{1}{72}\left[t_1\left(1+\frac{x_1}{2}\right) + t_2\left(1+\frac{x_2}{2}\right)\right]\rho_0\right\}, \quad (10)$$

where $\alpha = (3/5)\,(3\,\pi^2/2)^{2/3}$.

Similarly, for the isovector mode one has the coefficient $C_{\rm sym}$ of the isospin symmetry,

$$C_{\rm sym}(\rho_0) = \frac{5}{9}\alpha\frac{\hbar^2}{2m}\rho_0^{2/3} - \frac{t_0}{4}\left(x_0+\frac{1}{2}\right)\rho_0 - \frac{t_3}{24}\left(x_3+\frac{1}{2}\right)\rho_0^{\nu+1} + \frac{5}{9}\alpha\left(\frac{t_2}{2} + \frac{5t_2x_2 - 3t_1x_1}{8}\right)\rho_0^{5/3}, \quad (11)$$

and the isovector coefficient $F_{S,-}$ of the anomalous dispersion,

$$F_{S,-}(\rho_0) = \frac{1}{2}\eta\frac{\hbar^2}{2m} - \left[\frac{t_1}{24}\left(1+\frac{5x_1}{2}\right) + \frac{t_2}{18}\left(1+\frac{19x_2}{8}\right)\right]\rho_0. \quad (12)$$

Below, we present the results of the numerical calculations of the incompressibility coefficient $K(\rho_0)$ and the symmetry energy coefficient $C_{\rm sym}(\rho_0)$ for the SkM* [20], Sly203b [15], and the more modern KDE0v1 [23] Skyrme interactions. We note that the KDE0v1 interaction was determined by a fit to the extensive data on binding energies, charge radii of nuclei, single-particle spin-orbit splitting, and for the first time the inclusion of the radii of valence single-particle neutron orbits and the energies of the isoscalar giant monopole resonances in the nuclei. Also included in the fit are additional constraints, such as the Landau stability conditions, the positive derivative of the symmetry energy, $L = 3\rho\ dC_{\rm sym}/d\rho$ at large particle density ρ [24,25], and a minimal value for the enhancement factor κ of the energy-weighted sum rule of the isovector giant dipole resonance. It is important to point out that 240 Skyrme interactions, published in the literature, were analyzed by an independent group [26] for their ability to pass constraints relating to experimental data on the properties of nuclear matter and their derivatives, such as incompressibility coefficient K, symmetry energy coefficient $C_{\rm sym}$, and its slope L, effective-mass m^*/m, and observational data of neutron stars. Only the KDE0v1, LNS, NRPAR, SKRA, and SQMC700 interactions passed the test. These five interactions were then tested in Ref. [27] for their ability to reproduce binding energies and fission barriers of the nuclei. Only KDE0v1 passed the test. We add that, although Skyrme parametrizations are not expected, in general, to reproduce data for which they were not fitted, the neutron star and fission barrier data that are reproduced by the KDE0v1 interaction were not included in the fit. We note that, although the LNS, NRPAR, SKRA, and SQMC700 were fitted to a wide range of data for the equations of state, we have adopted the KDE0v1 interaction for its ability to reproduce properties of finite nuclei, a reasonable approximation for our purposes. In Table I we present the values of the Skyrme parameters for the SkM*, KDE0v1, and Sly230b interactions and the corresponding physical quantities of nuclear matter at saturation density $\rho_{\rm eq}$.

TABLE I. Values of the Skyrme parameters and the corresponding physical quantities of nuclear matter for the SkM*, KDE0v1, and Sly230b interactions.

Parameters	SkM*	KDE0v1	Sly230b
t_0 (MeV fm^3)	−2645.00	−2553.0843	−2488.91
t_1 (MeV fm^5)	410.00	411.6963	486.82
t_2 (MeV fm^5)	−135.00	−419.8712	−546.39
t_3 (MeV fm$^{3(1+\nu)}$)	15595.00	14603.6069	13777.0
x_0	0.0900	0.6483	0.8340
x_1	0.0000	−0.3472	−0.3438
x_2	0.0000	−0.9268	−1.0
x_3	0.0000	0.9475	1.3539
W_0 (MeV fm^5)	130.00	124.4100	122.69
ν	0.16667	0.1673	0.166667
E/A	15.78	16.23	15.972
K (MeV)	216.7	227.54	229.90
$\rho_{\rm eq}$ (fm^{-3})	0.160	0.165	0.160
m^*/m	0.79	0.74	0.695
$C_{\rm sym}$ (MeV)	30.03	34.58	32.01
L (MeV)	45.78	54.69	45.97
κ	0.53	0.23	0.25
$T_{\rm crit}$ (MeV)	14.62	14.74	14.67

Note that, in general, the transport coefficients K, $C_{\rm sym}$, and $F_{S,\pm}$ in the equations of motion (7) are temperature dependent. This can be seen in a transparent way by normalizing the density ρ_0 to the equilibrium density $\rho_{\rm eq}(T)$ and using the dimensionless ratio $\rho_0/\rho_{\rm eq}(T)$ as a variable. To avoid any misunderstanding, we point out that the particle density ρ_0 is an independent variable which is fixed by the Lagrange multiplier ξ in the variational Euler-Lagrange Eq. (2). In the case of $\xi = 0$ and zero-temperature $T = 0$, the variational Eq. (2) provides the actual equilibrium state with the saturation density $\rho_0 = \rho_{\rm eq}(T = 0)$. In a heated system at $T \neq 0$ and below the phase-separation point, the equilibrium density $\rho_{\rm eq}(T)$ is derived by the equilibrium condition for the pressure $P(\rho,T) = 0$, where $P(\rho,T) = \rho^2\partial F(\rho,T)/\partial\rho$ and $F(\rho,T)$ is the free energy. For higher temperatures above the point of the phase separation, the value of $\rho_{\rm eq}(T)$ is

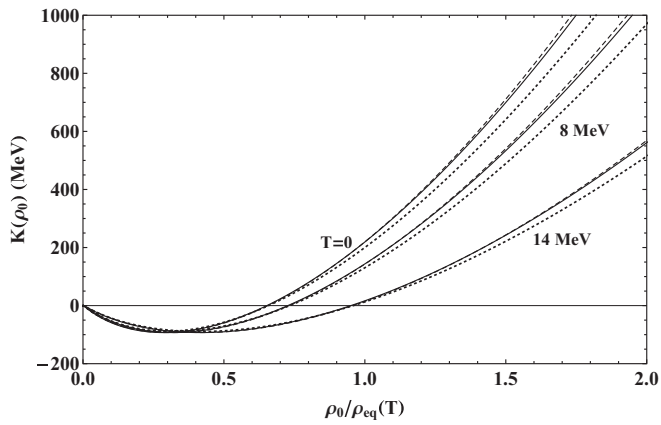

FIG. 1. The density dependence of the incompressibility coefficient $K(\rho_0)$ for different temperatures $T = 0$, 8, and 14 MeV (shown) for Skyrme interactions SkM* (dotted lines), KDE0v1 (solid lines), and SLy230b (dashed lines).

obtained from the interphase equilibrium condition [22]. The temperature dependence of the equilibrium density $\rho_{eq}(T)$ can be approximated as $\rho_{eq}(T) = \rho_{eq}(T = 0)(1 - 1.6 \times 10^{-3} T^2)$, where temperature T is taken in MeV, see Ref. [28]. In Figs. 1 and 2, we show the density dependence of the incompressibility K and the symmetry energy coefficient C_{sym}, respectively, for different temperatures T for three sets of Skyrme forces SkM*, KDE0v1, and Sly230b.

From Fig. 1, the instability regime where $K < 0$ is shifted to higher values of the ratio $\rho_0/\rho_{eq}(T)$ with increasing temperature T can be seen. The stable mode disappears at the critical temperature $T_{crit} = 14$ to 15 MeV where $K = 0$ at $\rho_0/\rho_{eq}(T) = 1$, see Table I.

Figure 2 shows that the dependence of the symmetry energy coefficient $C_{sym}(\rho_0)$ on the particle density ρ_0 is strongly sensitive to the choice of the Skyrme interactions. In contrast to the behavior of the incompressibility coefficient $K(\rho_0)$ in Fig. 1, the ρ dependence of the symmetry energy coefficient $C_{sym}(\rho_0)$ is completely different for the SkM*, KDE0v1, and Sly230b interactions. This fact was noted earlier in Ref. [14].

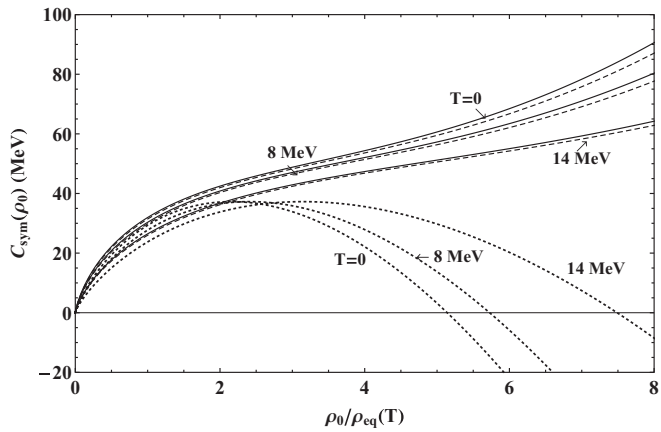

FIG. 2. The same as in Fig. 1 but for symmetry energy coefficient C_{sym}.

In the case of the SkM* interaction, the symmetry energy coefficient $C_{sym}(\rho_0)$ is a nonmonotonic function of the density, and it disappears in a superdense nuclear matter. In this case, the symmetry energy coefficient $C_{sym}(T)$ and thereby the isospin stability of Fermi liquid decreases with temperature for the dilute regime at $\rho_0/\rho_{eq}(T) \lesssim 1$. This behavior is reversed for the superdense regime at $\rho_0/\rho_{eq}(T) \gtrsim 2$. For the KDE0v1 and Sly230b interactions, the symmetry energy coefficient $C_{sym}(\rho_0)$ is an increasing function of particle density, and the nuclear matter does not reach the instability regime. Thus, the density dependence of the symmetry energy coefficient $C_{sym}(\rho_0)$ and the occurrence of the isospin instability are sensitive to the Skyrme interaction parametrization.

III. FERMI-SURFACE DISTORTION AND RELAXATION EFFECTS ON THE GROWTH OF BULK INSTABILITY

The solutions of the equations of motion (7) are significantly different for the stable and unstable modes. Focusing on the unstable modes $K < 0$ (or $C_{sym} < 0$), we introduce a growth rate of instability $\Gamma = -i\,\omega$ (Γ is real, $\Gamma > 0$) and obtain from Eqs. (7) the following dispersion relations:

$$\Gamma_{\pm}^2 = |u_{1,\pm}|^2\, q^2 - \zeta(\Gamma_{\pm})\, q^2 - \kappa_{s,\pm}\, q^4, \tag{13}$$

where $u_{1,+} = \sqrt{K/9m}$, $u_{1,-} = \sqrt{2C_{sym}/m}$, and $\kappa_{s,\pm} = (2/m)F_{S,\pm}$. In the case of the stable modes at $K > 0$ and $C_{sym} > 0$, the values $u_{1,+}$ and $u_{1,-}$ are the first sound velocities of the isoscalar and the isovector modes, respectively. The quantity $\zeta(\Gamma_{\pm})$ in Eq. (13) occurs due to the Fermi-surface distortion effect, and it is given by, see also Ref. [7],

$$\zeta(\Gamma_{\pm}) = \frac{4}{3m}\frac{\Gamma_{\pm}\tau_{\pm}}{1 + \Gamma_{\pm}\tau_{\pm}}\frac{P_0}{\rho_0}. \tag{14}$$

We have performed numerical calculations of the growth rate Γ_+ of the bulk instability for the Skyrme interaction KDE0v1. The relaxation time was taken in the form, see Ref. [29],

$$\tau_{\pm} = \hbar\beta_{\pm}/T^2, \tag{15}$$

with $\beta_+ = 9.2$, $\beta_- = 4.6$ MeV [30] and we have used $\eta = 4/9$ for Weizsäcker's correction in Eqs. (10) and (12). The bulk density ρ_0 of the unstable mode was taken as $\rho_0 = 0.3\,\rho_{eq}(T)$.

The nonmonotony behavior of the isoscalar instability growth rate $\Gamma_+(q)$ as a function of the wave-number q is caused by the anomalous dispersion term in Eq. (13). This term provides the stability with respect to the short-wavelength density fluctuations with increasing q. Comparing the dashed line and solid line 2 in Fig. 3, one concludes that the presence of the Fermi-surface distortion effects significantly reduces the instability. This fact was noted earlier in Ref. [7]. As seen from Fig. 3, the FSD effects are decreasing with increasing temperature T. This is due to the increase in the smearing of the Fermi surface with increasing T, and thereby the role of the Fermi-surface distortions becomes weaker with T. The left slopes of lines in Fig. 3 indicate the preference for nuclear multifragmentation [an increase in $\Gamma_+(q)$ with increasing q], whereas the right slopes are for the nuclear fission [an increase in $\Gamma_+(q)$ with decreasing q]. With increasing temperature, a point from the right slope of curve $\Gamma(q)$ can appear on its left

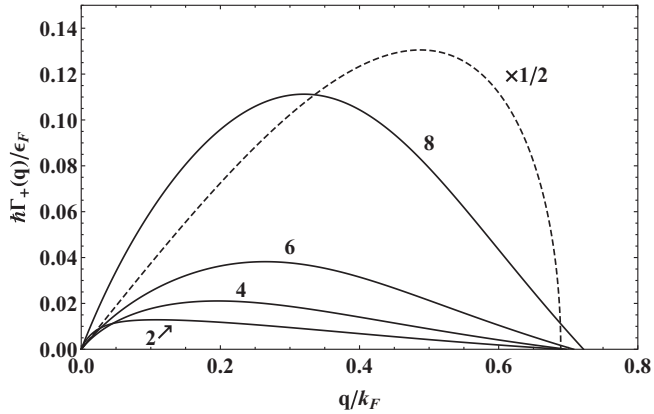

FIG. 3. The dependence of the isoscalar instability growth rate $\Gamma_+(q)$ on the wave-number q (in units of $k_F = p_F/\hbar$). The solid curves are for the Fermi liquid for different temperatures (shown near the solid curves in MeV) with bulk density $\rho_0 = 0.3\,\rho_{\rm eq}(T)$ and the relaxation parameter $\beta = 9.2$ MeV [see Eq. (15)]. The dashed line is the result for the nonviscous liquid without the Fermi-surface distortion effects at temperature $T = 2$ MeV. The calculations were performed for the KDE0v1 interaction.

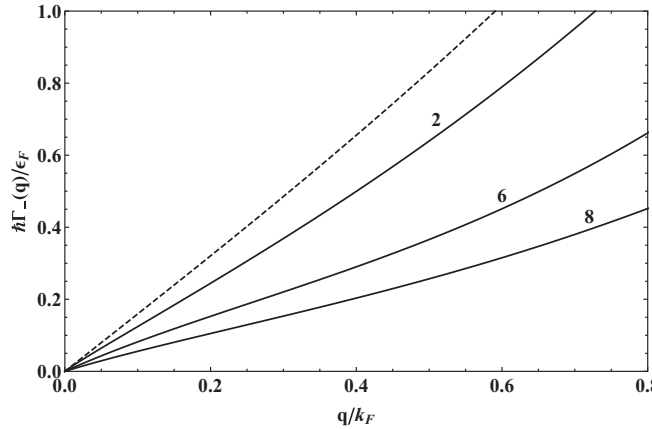

FIG. 4. The dependence of the isovector instability growth rate $\Gamma_-(q)$ on the wave-number q (in units of $k_f = p_F/\hbar$). The solid curves are for the Fermi liquid for different temperatures (shown near the solid curves in MeV) with bulk density $\rho_0 = 6\rho_{\rm eq}(T)$ and the relaxation parameter $\beta = 4.6$ MeV [see Eq. (15)]. The dashed line is the result for the nonviscous liquid without the Fermi-surface distortion effects at temperature $T = 2$ MeV. The calculations were performed for the SkM* interaction.

slope. Due to this fact, a nucleus which is unstable with respect to the fission mode at low-temperature T can become unstable for the multifragmentation mode at higher T.

Considering the isovector mode, we first note that, out of the three parametrizations of Skyrme-type interaction considered in this paper, an instability regime with $C_{\rm sym} < 0$ is reached in a superdense nuclear matter for the SkM* interaction (representing other interactions with a negative value of C_{sym} in a superdense matter). We add that the regime of superdense matter can be of interest, in particular, for astrophysics. The results of numerical calculations of the isovector growth rate $\Gamma_-(q)$ for the Skyrme interaction SkM* are shown in Fig. 4. As seen from Fig. 4, in contrast to Fig. 3 for $\Gamma_+(q)$, the isovector growth rate $\Gamma_-(q)$ in a superdense nuclear matter is a steadily increasing function of wave-number q. This is due to the fact that the coefficient of the anomalous dispersion $F_{S,-}$ in Eq. (7) changes sign from positive to negative in a superdense nuclear matter due to the presence of the term $\sim\rho_0$ in Eq. (12). Note also that the Fermi-surface distortions have little effect on the isovector growth rate $\Gamma_-(q)$ (compare the dashed and solid lines 2 in Fig. 4). This is similar to the case of zero sound modes in stable nuclear matter [8] where the Fermi-surface distortion effects do not strongly influence the characteristics of the isovector excitations.

The dispersion relation (13) also determines the critical value $q_{\pm,\rm crit}$ of the wave number which is given by the condition $\Gamma_\pm(q_{\pm,\rm crit}) = 0$. The presence of the critical value of wave-number $q_{\pm,\rm crit}$ plays an important role in the case of finite nuclei. For a finite nucleus the growth rate $\Gamma_+(q)$ depends on the multipolarity L of the density distortions $\delta\rho_\pm$ because wave-number $q = q_L$ is fixed by the boundary conditions which depend on the multipolarity L of the surface distortions [31,32]. Considering a finite nucleus, the dispersion relation (13) is completed by the boundary condition which can be taken similar to the classical form [31,32] as

$$m\,|u_+|^2\rho_0\,j_L(qR_0) = \,(L-1)\,(L+2)\,\sigma\,j_L'(qr)/q\,R_0^2\big|_{r=R_0}, \tag{16}$$

where R_0 is the nuclear radius, σ is the surface tension coefficient, and u_+ is the zero sound velocity, see Refs. [7,9]. The secular Eq. (16) gives the eigenvalue of the wave-number q_L, and the instability growth rate $\Gamma_+(q)$ depends on the position of q_L in the interval of $q = 0 - q_{\rm crit}$ [33].

The eigenvalues q_L of the secular Eq. (16) are temperature dependent because the surface tension coefficient σ in Eq. (16) is temperature dependent. In numerical calculations, we have used the following expression for $\sigma(T)$, (see Refs. [34,35]):

$$\sigma(T) = 1.1\left(\frac{T_{\rm crit}^2 - T^2}{T_{\rm crit}^2 + T^2}\right)^{5/4}\ {\rm MeV\ fm^{-2}}. \tag{17}$$

In Fig. 5 we have plotted the isoscalar instability growth rate $\Gamma_+(L)$ as a function of the multipolarity L of the particle density fluctuations for the nucleus of ^{208}Pb for different temperatures T. As seen from Fig. 5, the development of instability is significantly different for different temperature regimes. In the case of low temperatures (line $T = 0.5$), the preferable mode is the binary fission (low multipolarity $L = 2$ is most unstable). For higher temperatures (lines $T = 4$ and 8), the more preferable unstable modes are the ones with high multipolarity L which correspond to the multifragmentation of the small clusters. The number of clusters [the interval of accessible multipolarities L on the left slope of curve $\Gamma_+(L)$] increases with the further increasing temperature (compare lines 4, 6, and 8 MeV in Fig. 5). Note also that the modes with very high multipolarity L become overdamped having $\Gamma_+(L) < 0$. This is in agreement with the results of Fig. 3 and reflects the fact that the eigenvalues q_L are increasing with L.

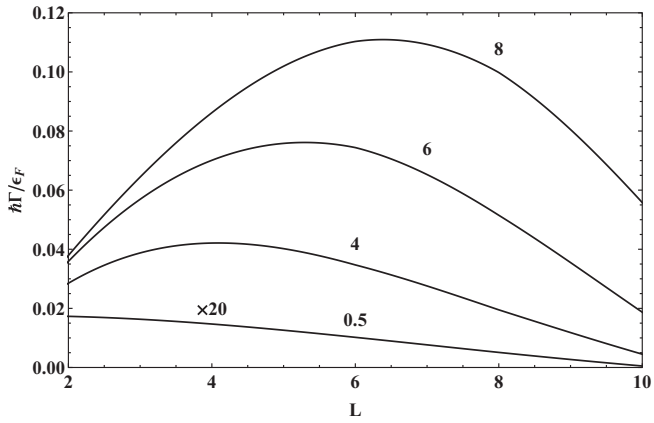

FIG. 5. The dependence of the isoscalar instability growth rate $\Gamma_+(L)$ on the multipolarity L of the particle density fluctuations for the nucleus of ^{208}Pb for different temperatures. $T = 0.5$, 4, 6, and 8 MeV, which are shown near the curves. The calculations were performed for the KDE0v1 interaction.

IV. SUMMARY AND CONCLUSIONS

We have considered the appearance and the development of instabilities in an asymmetric nuclear matter in both the isoscalar and the isovector channels. Our analysis is based on the equations of motion for the quantum Fermi liquid in the presence of the Fermi-surface distortion effects and the relaxation processes. We point out that a realistic description of the unstable modes in a homogeneous nuclear matter requires the extension of the equation of state by taking into consideration the gradient corrections for the total energy functional. The presence of the gradient corrections leads to the anomalous dispersion term in the equation of motion and significantly influences the behavior of the instability growth rate.

Studying the appearance of the bulk and isospin instabilities, we have performed numerical calculations of the dependence of the incompressibility coefficient $K(\rho_0)$ and the symmetry energy coefficient $C_{\rm sym}(\rho_0)$ on the nuclear density ρ_0. To evaluate the values of $K(\rho_0)$ and $C_{\rm sym}(\rho_0)$ at nonequilibrium density $\rho_0 \neq \rho_{\rm eq}$ we have applied the cranking approach. The external cranking field was used in the form which excludes the direct contribution of the cranking field to the incompressibility coefficient $K(\rho_0)$ for the Skyrme interactions SkM*, KDE0v1, and Sly230b for different temperatures and particle densities. We have established the critical temperature $T_{\rm crit} = 14$ to15 MeV where the nuclear matter becomes unstable at the equilibrium density $\rho_{\rm eq}(T)$. A peculiarity of the isovector mode is that the instability of the nuclear matter with respect to the isovector density fluctuation, i.e., regime $C_{\rm sym}(T) < 0$, can occur in the superdense nuclear matter only and depends significantly on the choice of the Skyrme interaction parametrization, such as in the case of SkM*.

We have shown that the Fermi-surface distortion effects strongly hinder the development of instabilities in nuclear matter. The dependence of the instability growth rate $\Gamma_+(q)$ on the wave-number q has a specific nonmonotonic behavior (see Figs. 3 and 5) which is caused by the anomalous dispersion term. Different slopes of the curve $\Gamma_+(q)$ reflect different regimes (fission or multifragmentation) of instability, see also Ref. [33]. To illustrate this fact, we have considered the behavior of the instability growth rate $\Gamma_+(q)$ in the finite nucleus of ^{208}Pb for different multipolarities L of particle density fluctuations and different temperatures T. The results presented in Fig. 5 show that the fission mode (low L) is preferable at low temperatures. The instability with respect to multifragmentation (high L) increases with temperatures. Moreover, one can expect that the yield of small fragments, which correspond to the highest values of L, is strongly increasing for high temperatures, see corresponding lines 4, 6, and 8 MeV in Fig. 5.

ACKNOWLEDGMENTS

This work was supported, in part, by the National Academy of Sciences of Ukraine under Grant No. CO-2-14/2016 (V.M.K.) and by the U.S. Department of Energy under Contract No. DOE-FG03-93ER40773 (S.S.). S.S. also thanks the Weizmann Institute of Science for support from the Weston Visiting Professorship Award and the nice hospitality extended to him.

APPENDIX: SKYRME ENERGY FUNCTIONAL

In this paper we use the ETFA for the kinetic energy of nucleons and the Skyrme potential energy due to the internucleon interactions. Assuming $\rho_- \ll \rho_+$ and using the standard form of the Skyrme interaction Eq. (3), we represent the total energy density $\epsilon_{\rm tot}[\rho_n, \rho_p]$ in the following form [20,36]:

$$\begin{aligned}\epsilon_{\rm tot}[\rho_+,\rho_-] = {}& \frac{\hbar^2}{2m}\alpha\rho_+^{5/3} + \frac{3}{8}t_0\rho_+^2 + \frac{1}{16}t_3\rho_+^{2+\nu} + \frac{1}{4}\left(\frac{3t_1+5t_2}{4} + t_2x_2\right)\alpha\rho_+^{8/3} \\ & + \left[\frac{\hbar^2}{2m}\frac{5}{9}\alpha\rho_+^{2/3} - \frac{t_0}{4}\left(x_0+\frac{1}{2}\right)\rho_+ - \frac{t_3}{24}\left(x_3+\frac{1}{2}\right)\rho_+^{1+\nu} + \frac{5}{9}\left(\frac{t_2}{2} + \frac{5t_2x_2 - 3t_1x_1}{8}\right)\alpha\rho_+^{5/3}\right]\frac{\rho_-^2}{\rho_+} + \frac{1}{4}\eta\frac{\hbar^2}{2m}\frac{(\nabla\rho_+)^2}{\rho_+} \\ & + \left[\frac{t_1}{12} - \frac{25}{144}t_2\left(1+\frac{4}{5}x_2\right)\right](\nabla\rho_+)^2 + \left[\frac{1}{4}\eta\frac{\hbar^2}{2m}\left(\frac{\Delta\rho_+}{\rho_+} - \frac{(\nabla\rho_+)^2}{\rho_+^2}\right) + \frac{1}{144}\left[t_1\left(1+\frac{x_1}{2}\right) + t_2\left(1+\frac{x_2}{2}\right)\right]\Delta\rho_+\right]\frac{\rho_-^2}{\rho_+} \\ & + \frac{1}{4}\eta\frac{\hbar^2}{2m}\frac{(\nabla\rho_-)^2}{\rho_+} - \left[\frac{t_1}{48}\left(1+\frac{5x_1}{2}\right) + \frac{t_2}{36}\left(1+\frac{19x_2}{8}\right)\right](\nabla\rho_-)^2. \end{aligned} \tag{A1}$$

Here, t_0, t_1, t_2, t_3, x_0, x_1, x_2, x_3, and ν are the parameters of the Skyrme interaction, and η is the free Weizsäcker parameter of the ETFA.

One can rewrite (A1) using the following notations in the form

$$\epsilon_{\rm tot}[\rho_+,\rho_-] = A_1(\rho_+) + A_2(\rho_+)\,\rho_-^2 + [B_1(\rho_+) + C_1(\rho_+,\rho_-)](\nabla\rho_+)^2 + B_2(\rho_+)(\nabla\rho_-)^2 + D_1(\rho_+,\rho_-)\nabla^2\rho_+, \tag{A2}$$

where

$$\begin{aligned}
A_1(\rho_+) &= \frac{\hbar^2}{2m}\alpha\rho_+^{5/3} + \frac{3}{8}t_0\rho_+^2 + \frac{1}{16}t_3\rho_+^{2+\nu} + \frac{1}{4}\left(\frac{3t_1+5t_2}{4} + t_2x_2\right)\alpha\rho_+^{8/3},\\
A_2(\rho_+) &= \frac{\hbar^2}{2m}\frac{5}{9}\alpha\rho_+^{-1/3} - \frac{t_0}{4}\left(x_0+\frac{1}{2}\right) - \frac{t_3}{24}\left(x_3+\frac{1}{2}\right)\rho_+^{\nu} + \frac{5}{9}\left(\frac{t_2}{2} + \frac{5t_2x_2-3t_1x_1}{8}\right)\alpha\rho_+^{2/3},\\
B_1(\rho_+) &= \frac{1}{4}\eta\frac{\hbar^2}{2m}\frac{1}{\rho_+} + \left[\frac{t_1}{12} - \frac{25}{144}t_2\left(1+\frac{4}{5}x_2\right)\right],\\
B_2(\rho_+) &= \frac{1}{4}\eta\frac{\hbar^2}{2m}\frac{1}{\rho_+} - \left[\frac{t_1}{48}\left(1+\frac{5x_1}{2}\right) + \frac{t_2}{36}\left(1+\frac{19x_2}{8}\right)\right],\\
D_1(\rho_+,\rho_-) &= \frac{1}{4}\eta\frac{\hbar^2}{2m}\frac{\rho_-^2}{\rho_+^2} + \frac{1}{144}\left[t_1\left(1+\frac{x_1}{2}\right) + t_2\left(1+\frac{x_2}{2}\right)\right]\frac{\rho_-^2}{\rho_+},\\
C_1(\rho_+,\rho_-) &= -\frac{1}{4}\eta\frac{\hbar^2}{2m}\frac{\rho_-^2}{\rho_+^3}.
\end{aligned} \tag{A3}$$

Using $\epsilon_{\rm tot}[\rho]$ of the form of Eq. (A2), one can evaluate the functional derivatives $\delta E/\delta\rho_\pm$ for the equations of motion (4), which are significantly different for the isoscalar and isovector modes.

(i) Isoscalar mode,

$$\begin{aligned}
\frac{\delta E}{\delta\rho_+} &= \frac{\partial}{\partial\rho_+}A_1(\rho_+) + \rho_-^2\frac{\partial}{\partial\rho_+}A_2(\rho_+) + (\nabla\rho_+)^2\frac{\partial}{\partial\rho_+}[B_1(\rho_+) + C_1(\rho_+,\rho_-)]\\
&\quad + (\nabla\rho_-)^2\frac{\partial}{\partial\rho_+}B_2(\rho_+) + \left(\nabla^2\rho_+\right)\frac{\partial}{\partial\rho_+}D_1(\rho_+,\rho_-) - 2\nabla[B_1(\rho_+) + C_1(\rho_+,\rho_-)]\nabla\rho_+ + +\nabla^2 D_1(\rho_+,\rho_-),\\
\frac{\delta E}{\delta\rho_+} &= \left(\frac{\delta E}{\delta\rho_+}\right)_{\rho_0} + \left(\frac{\partial^2 A_1}{\partial\rho_+^2}\right)_{\rho_0}\delta\rho_+ + \left(\rho_-^2\frac{\partial^2 A_2}{\partial\rho_+^2}\right)_{\rho_0}\delta\rho_+ + \left(\frac{\partial(B_1+C_1)}{\partial\rho_+}\right)_{\rho_0}(\nabla\delta\rho_+)^2\\
&\quad + \left(\frac{\partial D_1}{\partial\rho_+}\right)_{\rho_0}\nabla^2\delta\rho_+ - 2\nabla\left(\frac{\partial(B_1+C_1)}{\partial\rho_+}\right)_{\rho_0}\delta\rho_+\cdot(\nabla\rho_+)_0 - 2\nabla[B_1(\rho_+) + C_1(\rho_+,\rho_-)]_{\rho_0}\cdot\nabla\delta\rho_+\\
&\quad - 2\left(\frac{\partial(B_1+C_1)}{\partial\rho_+}\right)_{\rho_0}\delta\rho_+\left(\nabla^2\rho_+\right)_0 - 2\{[B_1(\rho_+) + C_1(\rho_+,\rho_-)]\}_{\rho_0}\nabla^2\delta\rho_+ + \left(\frac{\partial D_1}{\partial\rho_+}\right)_{\rho_0}\nabla^2\delta\rho_+,\\
\frac{\delta E}{\delta\rho_+} &= \left(\frac{\delta E}{\delta\rho_+}\right)_{\rho_0} + \left[\left(\frac{\partial^2 A_1}{\partial\rho_+^2}\right)_{\rho_0} + \left(\rho_-^2\frac{\partial^2 A_2}{\partial\rho_+^2}\right)_{\rho_0}\right]\delta\rho_+ + \left[2\left(\frac{\partial D_1}{\partial\rho_+}\right)_{\rho_0} - 2\{[B_1(\rho_+) + C_1(\rho_+,\rho_-)]\}_{\rho_0}\right]\nabla^2\delta\rho_+.
\end{aligned} \tag{A4}$$

(ii) Isovector mode,

$$\begin{aligned}
\frac{\delta E}{\delta\rho_-} &= 2\,A_2(\rho_+)\,\rho_- + (\nabla\rho_+)^2\frac{\partial}{\partial\rho_-}C_1(\rho_+,\rho_-) + (\nabla^2\rho_+)\frac{\partial}{\partial\rho_-}D_1(\rho_+,\rho_-) - 2\nabla B_2(\rho_+)\,\nabla\rho_-,\\
\frac{\delta E}{\delta\rho_-} &= \left(\frac{\delta E}{\delta\rho_-}\right)_{\rho_0} + 2\,[A_2(\rho_+)]_0\delta\rho_- + \left((\nabla\rho_+)^2\frac{\partial^2}{\partial\rho_-^2}C_1(\rho_+,\rho_-)\right)_{\rho_0}\delta\rho_- + \left((\nabla\rho_+)^2\frac{\partial^2}{\partial\rho_-^2}D_1(\rho_+,\rho_-)\right)_{\rho_0}\delta\rho_-\\
&\quad - 2[\nabla B_2(\rho_+)]_{\rho_0}\cdot\nabla\delta\rho_- - 2[B_2(\rho_+)]_{\rho_0}\nabla^2\rho_-\frac{\delta E}{\delta\rho_-} = \left(\frac{\delta E}{\delta\rho_-}\right)_{\rho_0} + 2[A_2(\rho_+)]_{\rho_0}\delta\rho_- - 2[B_2(\rho_+)]_{\rho_0}\nabla^2\rho_-.
\end{aligned} \tag{A5}$$

We note that the first terms on the right-hand sides of Eqs. (A4) and (A5) do not contribute to the equation of motion (4) because of the variational condition (2) and the chemical potentials $\mu_\pm = \text{const}$, namely,

$$\mu_+ = \left.\frac{\partial E}{\partial A}\right|_V = \left(\frac{\delta E}{\delta \rho_+}\right)_{\rho_0} = \text{const}, \quad \mu_- = \left.\frac{\partial E}{\partial (N-Z)}\right|_V = \left(\frac{\delta E}{\delta \rho_-}\right)_{\rho_0} = \text{const}. \tag{A6}$$

[1] H. Heiselberg, C. J. Pethick, and D. G. Ravenhall, Ann. Phys. (NY) **223**, 37 (1993).
[2] M. Colonna, P. Chomaz, and J. Randrup, Nucl. Phys. A **567**, 637 (1994).
[3] M. Colonna and P. Chomaz, Phys. Rev. C **49**, 1908 (1994).
[4] J. Konopka, H. Graf, H. Stöcker, and W. Greiner, Phys. Rev. C **50**, 2085 (1994).
[5] H. Müller and B. D. Serot, Phys. Rev. C **52**, 2072 (1995).
[6] V. Baran, M. Colonna, M. Di Toro, and A. B. Larionov, Nucl. Phys. A **632**, 287 (1998).
[7] V. M. Kolomietz and S. Shlomo, Phys. Rev. C **60**, 044612 (1999).
[8] V. M. Kolomietz and S. Shlomo, Phys. Rev. C **64**, 044304 (2001).
[9] V. M. Kolomietz and S. Shlomo, Phys. Rep. **390**, 133 (2004).
[10] B. Jacquot, M. Colonna, S. Ayik, and P. Chomaz, Nucl. Phys. A **617**, 356 (1998).
[11] A. Lejeune, P. Grange, M. Martzolf, and J. Cugnon, Nucl. Phys. A **453**, 189 (1986).
[12] J. Cugnon, A. Lejeune, M. Baldo, and U. Lombardo, Nucl. Phys. A **492**, 173 (1989).
[13] T. H. R. Skyrme, Nucl. Phys. **9**, 615 (1959).
[14] E. Chabanat, P. Bonche, P. Haensel, J. Meyer, and R. Schaeffer, Nucl. Phys. A **627**, 710 (1997).
[15] E. Chabanat, R Bonche, R Haensel, J. Meyer, and R. Schaeffer, Nucl. Phys. A **635**, 231 (1998).
[16] J. R. Nix and A. J. Sierk, Phys. Rev. C **21**, 396 (1980).
[17] D. Kiderlen, V. M. Kolomietz, and S. Shlomo, Nucl. Phys. A **608**, 32 (1996).
[18] D. A. Kirzhnitz, *Field Theoretical Methods in Many Body Systems* (Pergamon, London, 1967).
[19] P. Ring and P. Schuck, *The Nuclear Many-Body Problem* (Springer-Verlag, New York, 1980), Chap. 13.
[20] M. Brack, C. Guet, and H.-B. Håkansson, Phys. Rep. **123**, 275 (1985).
[21] M. Di Toro, V. M. Kolomietz, and A. B. Larionov, Phys. Rev. C **59**, 3099 (1999).
[22] L. D. Landau and E. M. Lifshitz, *Statistical Physics* (Pergamon, Oxford, 1958).
[23] B. K. Agrawal, S. Shlomo, and V. K. Au, Phys. Rev. C **72**, 014310 (2005).
[24] C. J. Horowitz and J. Piekarewicz, Phys. Rev. C **66**, 055803 (2002).
[25] J. R. Stone, J. C. Miller, R. Koncewicz, P. D. Stevenson, and M. R. Strayer, Phys. Rev. C **68**, 034324 (2003).
[26] M. Dutra, O. Lourenço, J. S. Sá Martins, A. Delfino, J. R. Stone, and P. D. Stevenson, Phys. Rev. C **85**, 035201 (2012).
[27] P. D. Stevenson, P. D. Goddard, J. R. Stone, and M. Dutta, *Do Skyrme Forces that Fit Nuclear Matter Work Well in Finite Nuclei?* AIP Conf. Proc. No. 1529 (AIP, New York, 2012), p. 262.
[28] S. Shlomo and V. M. Kolomietz, Rep. Prog. Phys. **68**, 1 (2005).
[29] A. A. Abrikosov and I. M. Khalatnikov, Rep. Prog. Phys. **22**, 329 (1959).
[30] V. M. Kolomietz, V. A. Plujko, and S. Shlomo, Phys. Rev. C **54**, 3014 (1996).
[31] H. Lamb, *Hydrodynamics* (Dover, New York, 1945).
[32] A. Bohr and B. R. Mottelson, *Nuclear Structure* (Benjamin, New York, 1975), Vol. 2, Chap. 6.
[33] C. J. Pethick and D. G. Ravenhall, Nucl. Phys. A **471**, 19c (1987); Ann. Phys. (NY) **183**, 131 (1988).
[34] D. G. Ravenhall, C. J. Pethick, and J. M. Lattimer, Nucl. Phys. A **407**, 571 (1983).
[35] V. M. Kolomietz, A. I. Sanzhur, S. Shlomo, and S. A. Firin, Phys. Rev. C **64**, 054315 (2001).
[36] V. M. Kolomietz and A. I. Sanzhur, Eur. Phys. J. A **38**, 345 (2008).